ABSTRACT

Title of dissertation: Direct measurement of a Feshbach resonance with imaging and measuring topology of BECs in a synthetic dimensions

Dina Genkina
Doctor of Philosophy, 2018

Dissertation directed by: Professor Ian Spielman
Department of Physics

Direct measurement of a Feshbach resonance with imaging of s-wave scattering and measuring topology of BECs in a synthetic dimensions lattice

by

Dina Genkina

Dissertation submitted to the Faculty of the Graduate School of the
University of Maryland, College Park in partial fulfillment
of the requirements for the degree of
Doctor of Philosophy
2018

Advisory Committee:
Professor Ian Spielman, Chair/Advisor

Chapter 2: Absorption imaging in the presence of strong recoil induced detuning

2.1 Near-resonant atom-light interaction

In this section, we will assume the atom can be treated as a two-level system: one with a ground and excited atomic state, with an energy difference of energy difference $\hbar\omega_0$. When such an atom, starting in the ground state, is illuminated by a laser beam with frequency $\hbar\omega_{\mathrm{L}}$, there are three kinds of transitions that occur: during aborption the atom aborbs a photon from the laser and goes from the ground to the excited state; during stimulated emission, the atom emits a photon into the field of the laser beam and jump from the excited to the ground state; during spontaneous emission, the atom decays to the ground state from the excited state with no help from the laser, emitting into a random vacuum mode. Stimulated emission results in coherent light co-propagating with the laser beam, while spontaneous emission results in light scattering incoherently in any direction. The rate of spontaneous emission from an excited state is given by the natural transition linewidth of the transition Γ.

On timescales short compared to $1/\Gamma$, spontaneous emission can be ignored, and an atom undergoes coherent Rabi oscillations between the ground and excited states via cycles of absorption and stimulated emission [1]. Taking c_g and c_e to be the time-dependent coefficients multiplying the eigen state wavefuntions of the ground and excited state respectively, and assuming the atom starts in the ground state $c_g(t=0)=1$, the excited state population is given by

$$c_e(t) = -i\frac{\Omega}{\Omega'} sin\left(\frac{\Omega' t}{2}\right) e^{-i\delta t/2}, \tag{2.1}$$

where Ω is the Rabi frequency given by $SOMETHINGINTERMSOFINTENSITY$, $\Omega' = \sqrt{\Omega^2 + \delta^2}$ is the generalized Rabi frequency and $\delta = \omega_0 - \omega_{\mathrm{L}}$ is the detuniong of the laser from atomic resonance.

In the regime where spontaneous emission cannot be ignored, Rabi oscillations of each individual atom are intermittently interrupted by decay to the ground state. Averaging over an atomic ensamble, on the time scale of a single Rabi oscillation the overall excited state population reaches a steady state, and the rate of spontaneous emission becomes constant. Since during spontaneous emission the ejected photon can go into any vacuum mode, this process can be thought of as the scattering of

photons by the atoms. This scattering rate is given by [1]

$$\gamma_{\mathrm{sc}} = \frac{\Gamma}{2} \frac{I/I_{\mathrm{sat}}}{1 + 4(\delta/\Gamma)^2 + I/I_{\mathrm{sat}}}, \tag{2.2}$$

where I_{sat} is the saturation intensity. This is the intensity at which the timescale of spontaneous emission matches the Rabi oscillation rate, reducing the capacity for absorption of extra light.

2.2 Absorption imaging

Absorption imaging takes advantage of the on-resonant interaction described in the previous section. An on or near-resonant laser beam ($\delta/\Gamma \ll 1$) is shined at the atoms, and the aborbed light acts to create a shadow in the shape of the atoms in the laser beam. This beam with the shadow is then imaged on a camera, in our case a CCD, as depicted in Figure 1a (top). This is called the atom image, and the intensity distribution over the camera is denoted by $I_f(x, y)$, where the subscript f stands for final - the intensity after the light has encountered the atoms. To quantify the 'shadowed out' intensity, after the atoms have left the trap the same laser intensity is shined directly at the camera, as in Figure 1a (bottom). This is called the probe image, and the intensity distribution over the camera is denoted by $I_0(x, y)$, where the subscript 0 indicated initial - the intensity before the light had encountered the atoms.

To recover the atom number distribution encountered by the light, consider an atomic cloud with 3D density $\rho(x, y, z)$. Since we can only obtain 2D information from the camera, we can only hope to recover a 2D atomic column density $n(x, y) = \int \rho(x, y, z)\mathrm{d}z$. Focusing in on a single pixel of the camera, we can consider a single value of I_0 and I_f to recover a local n. As the laser light propagates through the atomic cloud, the intensity of the light will diminish due to absorption. This absorption as a function of propagation direction z can be expressed using the scattering rate equation Eq. 2.2 as the number of photons scattered by the atoms (proportional to the atomic density times the scattering rate) times the photon energy $\hbar\omega_{\mathrm{L}}$:

$$\frac{d}{dz}\frac{I(z)}{I_{\mathrm{sat}}} = -\hbar\omega_{\mathrm{L}}\rho(z)\gamma_{sc}(z) = -\rho(z)\sigma_0 \frac{I(z)/I_{\mathrm{sat}}}{1 + 4\delta^2/\Gamma^2 + I(z)/I_{\mathrm{sat}}}, \tag{2.3}$$

where the resonant scattering cross section is $\sigma_0 = 3\lambda_0^2/2\pi$, and λ_0 is the wavelength asociatted with atomic resonance.

Integrating both sides of Eq. 2.3, we obtain

$$\sigma_0 n = \left(1 + 4\delta^2/\Gamma^2\right) \ln(I_0/I_f) + \left(I_0 - I_f\right)/I_{\mathrm{sat}}. \tag{2.4}$$

The quantity $OD = ln(I_0/I_f)$ is called the optical depth of the cloud. When the probe intensity I_0 is much smaller than the saturation intensity, the second term in Eq. 2.4 becomes negligible. Assuming further that the probe light is on resonance,

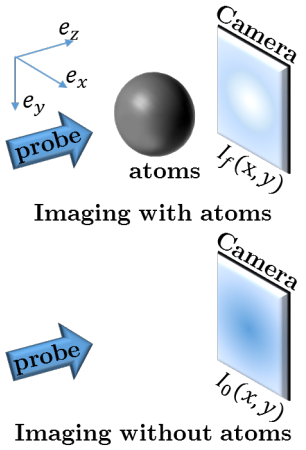

(a)

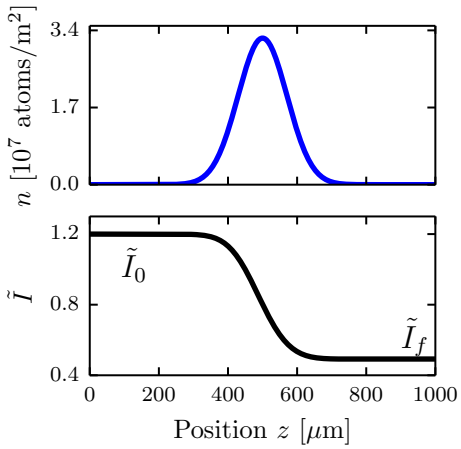

(b)

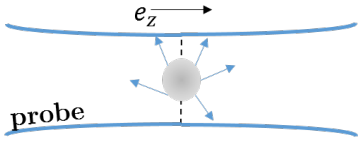

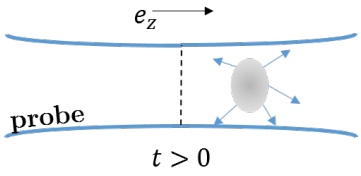

(c)

Figure 1: Absorption imaging. (a) Near resonant probe light illuminates the atoms, and the transmitted light (containing a shadow of the atoms) is imaged on the camera. A second image taken with no atoms provides a reference. (b) The probe beam is partially absorbed as it traverses the cloud, and the intensity seen by atoms further along the imaging direction $e_\mathbf{z}$ is lowered. (c) An atomic cloud illuminated by a probe light field absorbs photons from the probe and re-emits them in all directions. This process results in a net acceleration of the cloud in the direction of the probe light as well as diffusive spreading in the transverse directions.

$\delta = 0$, the atomic column density becomes simply $\sigma_0 n = OD$. Figure 1b shows a Gaussian atomic density distribution (top) and the resulting probe intensity as a function of position in the cloud (bottom). The intensity drops from its initial to final value gradually as it traverses the cloud.

However, there is an important effect that the above equations do not account for. Namely, as the atoms absorb light from the probe beam, they also get a momentum kick equal to the momentum of a photon during each collision $\hbar k_r = h/\lambda_L$ in the direction of propagation. It is true that the absorbed photon will then be re-emitted by the atom, inducing a loss of momentum, but since this happens through the process of spontaneous emission into a random vacuum mode, the average momentum kick acquired this way over many re-emissions will average to zero. On average, each photon absorbed will induce a change in velocity of the atom of $v_r = \hbar k_r/m$, where m is the atomic mass, as depicted in Fig. 1c. As the velocity of the atom changes, due to the Doppler effect, the apparent laser frequency will change as well. Therefore, even if the laser light is exactly on-resonant for a stationary atom, it will become off-resonant for longer imaging times, and Eq. 2.3 will acquire a time dependence. For most experiments, this effect is small and can be neglected. However, if the imaging time becomes of order a recoil time t_r, a time after which the recoil-induced detuning δ becomes of order Γ, this effect becomes significant. We explore this effect in the following sections.

2.3 Recoil-induced detuning

After absorbing a number of photons N, an atom will obtain a recoil velocity of Nv_r. Via the Doppler effect, this will result in a detuning $\delta = Nk_\mathrm{r}v_\mathrm{r}$. This detuning will increase as more atoms are absorbed, and therefore depend on time, making the absorbed intensity also time dependent. We can generalize Eq. 2.3 to include a time dependence on the detuning term and therefore also the intensity:

$$\frac{d}{dz}\frac{I(z,t)}{I_\mathrm{sat}} = -\rho(z)\sigma_0\frac{I(z,t)/I_\mathrm{sat}}{1+4\delta(z,t)^2/\Gamma^2 + I(z,t)/I_\mathrm{sat}}. \tag{2.5}$$

The number of photons absorbed per atom will depend on the intensity lost, up until the current time, at that location. The detuning will therefore be proportional to the total number of photons lost up until time t at that location, proportional to the absorbed intensity divided by the single photon energy $\hbar\omega_L$, divided by the number of atoms that participated in the aborption $\rho(z)$ times the detuning $k_\mathrm{r}v_\mathrm{r}$:

$$\delta(t,z) = \frac{k_\mathrm{r}v_\mathrm{r}}{\hbar\omega_L\rho(z)}\int_0^t \frac{dI(z,\tau)}{dz}\mathrm{d}\tau. \tag{2.6}$$

These equations are interdependent, and cannot be in general solved analytically.

Figure 2a shows the velocity and detuning as a function of position in space for three different imaging times, calculated numberically. All calculations in this chapter were done for a cloud of ^{4}0K atoms, as that is relevant to our experiment described in the next chapter. The resonant wavelength is $PUTALLNUMBERSFORKINHERE$

2.4 Perturbative treatment

We can treat these equations perturbatively in time. To first order, we can set the detuning in Eq. 2.5 to $\delta = 0$, assume $I(z)$ is time independent, and plug that into Eq. 2.6 to obtain

$$\delta(t,z) = \frac{k_r v_r}{\hbar\omega_L \rho(z)} \int_0^t -\rho(z)\sigma_0 \frac{I(z)}{1+I(z)/I_{sat}} d\tau \tag{2.7}$$

$$= \frac{k_r v_r \sigma_0}{\hbar\omega_L} \frac{I(z)}{1+I/I_{sat}} t. \tag{2.8}$$

This can then be recursively plugged into Eq. 2.5 to obtain

$$\frac{d}{dz}\frac{I(z,t)}{I_{sat}} = -\rho(z)\sigma_0 \frac{I(z,t)/I_{sat}}{1+4\left(\frac{k_r v_r \sigma_0}{\hbar\omega_L \Gamma}\frac{I(z)}{1+I/I_{sat}}\right)^2 t^2 + I(z,t)/I_{sat}}. \tag{2.9}$$

Integrating both sides of the above equation, we obtain a perturbative equation to second order in time [4]:

$$\sigma_0 n = ln(I_0/I_f) + \frac{I_0 - I_f}{I_{sat}} + \frac{(k_r v_r t)^2}{3}\left(\frac{I_{sat}}{I_f + I_{sat}} - \frac{I_{sat}}{I_0 + I_{sat}} + \ln\left(\frac{I_f + I_{sat}}{I_0 + I_{sat}}\right)\right). \tag{2.10}$$

In Fig. 2b, we examine for what imaging times the above perturbative equation, as well as the modelt that completely ignores recoil induced detuning, is valid. We do this by performing numerical simulations to extract a value for the final intensity I_f and using Eq. **??** and Eq. 2.10 to extract values $\sigma_0 n$ that would be deduced from experimnet. We find that within the recoil time, both analytic expressions start to differ from the true atomic column density by over 5%, and the perturbative model of Eq. 2.10 quickly divereges thereafter.

In the following sections, we describe two versions of numerical simulations that we have performed in order to appropriately extract atomic column densities from experimental data.

2.5 Stationary atom model

To solve Eqs. (2.5)-(2.6), we divided the cloud into spatial bins. In this approximation, the number of atoms in each bin was time-independent. The algorithm used is shown in Alg. (1), in which we took a Gaussian profile for our initial density distribution. We call the optical depth simulated by this algorithm the simulated optical depth OD^{sim1}.

We checked the validity of our simulation in the limits where the problem is analytically solvable. In the limit where the probe intensity is much weaker than the saturation intensity, $\tilde{I}_0 \ll 1$, the atoms' velocities are hardly changed, and Eq.(2.5) reduces to

$$\frac{d\tilde{I}(z)}{dz} = -\rho\sigma_0 \tilde{I}(z), \text{ from which we recover the analytic form} \tag{2.11}$$

$$\sigma_0 n^{(0)} = -\ln \tilde{I}_0/\tilde{I}_f. \tag{2.12}$$

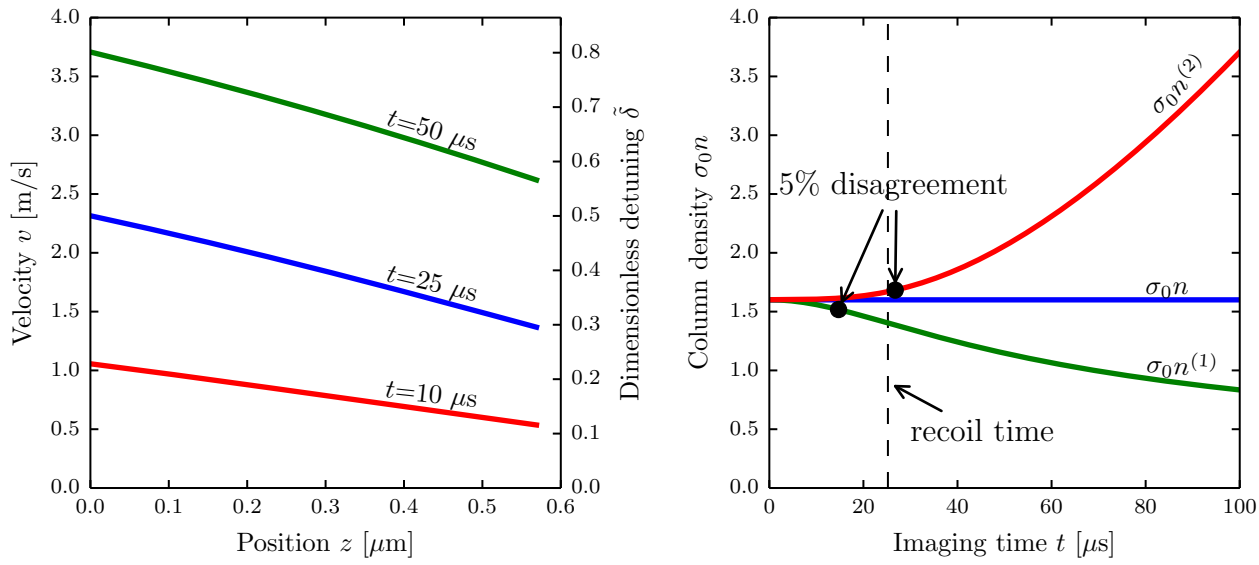

(a) (b)

Figure 2: (a) Dependence of velocity and detuning on position simulated for ^{40}K at three different imaging times and a probe intensity $\tilde{I}_0 = 0.8$. (b) Column densities deduced from optical depths obtained from recoil detuning corrected simulation of on-resonant imaging of ^{40}K atoms at probe intensity $\tilde{I}_0 = 0.8$. The input column density $\sigma_0 n = 1.6$. $\sigma_0 n^{(1)}$ is the high probe intensity corrected column density given by Eq. (2.4). $\sigma_0 n^{(2)}$ is the column density as expanded to second order in time, Eq. (**??**).

Algorithm 1 Stationary atom model

$I[n = 0, t] = I_0$ {n is the bin index, t is the time index, I is in units of $I_{\rm sat}$}
$\delta[n, t = 0] = 0$ {light initially resonant, δ in units of $\Gamma/2$}
$H_f = 0$ {Radiant fluence seen by camera after passing through cloud}
for $t = 0$ to t_f **do** {loop over time steps}
  for $n = 1$ to N **do** {loop over bins, N is total bin number}
    $A = \sigma_0 \rho[n] dz$ {dz is the size of spatial step}
    $B = v_{\rm r} dt/(\hbar c \rho[n])$ {dt is the size of the time step}
    $I[n, t] = I[n-1, t] - AI[n-1, t]/(1 + \delta[n, t-1]^2 + I[n-1, t])$ {Eq. (2.5)}
    $\delta[n, t] = \delta[n, t-1] + B\,(I[n-1, t] - I[n, t])$ {Eq. (2.6)}
  end for
  $H_f = H_f + I[N, t] dt$ {collecting total fluence seen by the camera}
end for
$OD^{\rm sim1} = -\ln(H_f/I_0 t_f)$

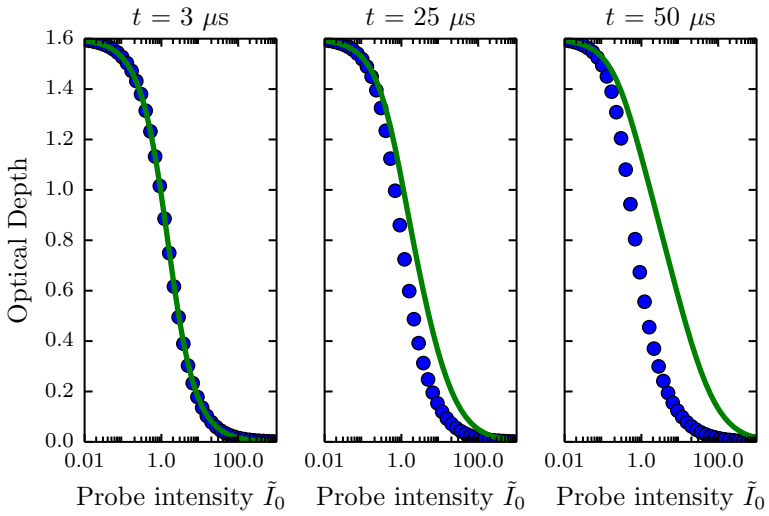

Figure 3: Optical depth as a function of probe intensity as predicted by the simulation (blue symbols) and by Eq. (2.4) (green curves), for three different imaging times. As expected, the predictions agree in both the high and low intensity limits, and differ for probe intensities comparable to the saturation intensity and longer imaging times.

In the limit where the probe intensity is much larger than the saturation intensity, $\tilde{I}_0 \gg \tilde{\delta}$, even far detuned atoms will scatter light at their maximum rate. The time dependence of the detuning can thus be neglected, and Eq. (2.5) becomes

$$\frac{d\tilde{I}(z)}{dz} = -\rho\sigma_0, \text{ which integrates to} \tag{2.13}$$

$$\sigma_0 n = \tilde{I}_0 - \tilde{I}_f. \tag{2.14}$$

We recognize the right hand sides of Eq. (2.12) and Eq. (2.14) as the two terms in Eq. (2.4). Thus, as shown in Fig. 3, OD^{sim1} coincides with the optical depth as predicted by Eq. (2.4) in both the small and large probe intensity limits.

We used the results of this simulation to check the self-consistency of the stationary atom assumption, i.e. the distance traveled by the atoms (as deduced from integrating the acquired recoil velocity over the imaging time) is less than the bin size. As can be seen from Fig. 4(a), not only do the atoms travel more than the bin size, but they travel far beyond the initial extent of the cloud. Moreover, owing to the higher initial scatter rate, the back of the cloud overtakes the front for long imaging times. Thus, the atomic distribution as a function of position changes dramatically during the imaging pulse, and the stationary assumption is invalid.

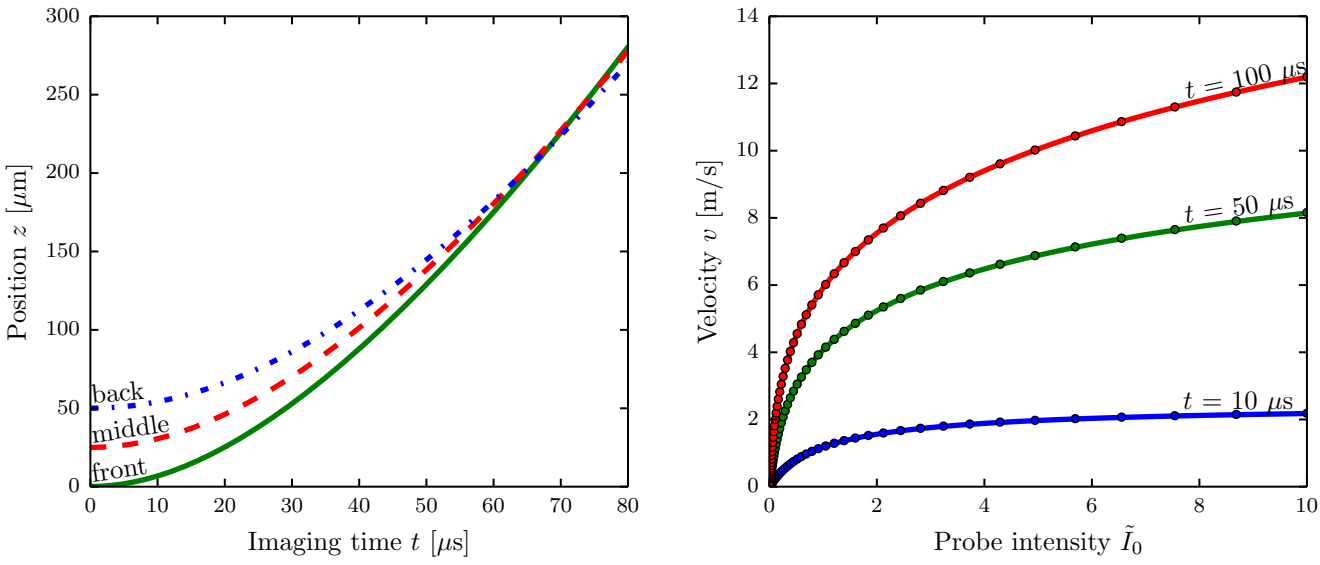

(a) (b)

Figure 4: (a) Position of atoms as a function of imaging time for atoms in the first (solid green), middle (dashed red), and last (dotted blue) bins of the simulated density distribution for an initial cloud 50 μm in extent. The probe intensity used in this calculation was $1.2\, I_{\rm sat}$, and the column density was $\sigma_0 n = 1.6$. (b) The velocity of a single composite atom as a function of probe intensity for various imaging times. Simulation data (dots) and numerical solutions of Eq. (2.15) (lines) are in agreement.

2.6 Traveling atom model

To account for the changing atomic distribution during the imaging pulse, we numerically simulated the classical kinetics of atoms subject to the recoil driven optical forces. To simulate large ensembles in a reasonable time, we modeled composite atoms, each describing the aggregate behavior of N_{ca} atoms. The amended algorithm is shown in Alg. (2).

Algorithm 2 Travelling atom model

$z[n] = z_0$, $\delta[n] = 0$ {initialize position and detuning for each composite atom, labeled by index n}
$O[i] = n$ {make a list of composite atom indexes, ordered by position}
$I[n = 0, t] = I_0$ { t is the time index, I is in units of I_{sat}}
$H_f = 0$ {Radiant fluence seen by camera after passing through cloud}
for $t = 0$ to t_f **do** {loop over time steps}
  for $i = 1$ to N **do** {loop over superatoms}
    $n = O[i]$ {apply probe intensity to composite atoms in order of appearance}
    $A = \sigma_0 N_{sa} dz$ {dz is length over which atoms were grouped into single composite atom}
    $B = v_{\mathrm{r}} dt/(\hbar c N_{sa})$ {dt is the time step}
    $I[n, t] = I[n-1, t] - AI[n-1, t]/(1 + \delta[n]^2 + I[n-1, t])$ {Eq. (2.5)}
    $\delta[n]$ += $B\,(I[n-1, t] - I[n, t])$ {Eq. (2.6), detuning in units of $\Gamma/2$}
    $z[n]$ += $dt\Gamma\delta/2k$ {k is the wavenumber, $\Gamma\delta/2k$ is the velocity at δ detuning}
  end for
  $O[i]$=sort(n, key =$z[n]$) {sort composite atom indexes by current position}
  $H_f H_f + I[N, t]dt$ {collecting total fluence seen by the camera}
end for
$OD^{\mathrm{sim2}} = -\ln(H_f/I_0 t_f)$

To validate our code, we again checked the velocity predicted in this model against known limits. One such limit is that of a single composite atom. In this case, there is no attenuation, and the intensity seen by the composite atom is constant at $\tilde{I}_0$. Only the detuning evolves in time, and Eqs. (2.5) and (2.6) give

$$\frac{d\tilde{\delta}(t)}{dt} = \frac{k_{\mathrm{r}} v_{\mathrm{r}}}{2} \frac{\tilde{I}}{1 + 4\tilde{\delta}^2 + \tilde{I}}. \tag{2.15}$$

Equation (2.15) can be solved numerically, and is in agreement with our simulation, as seen in Fig. 4(b).

We used this model to study the time evolution of the cloud shape during imaging and visualized the phase space evolution of superatoms, shown in Fig. 5. The cloud is strongly distorted during imaging.

We compared the optical depths predicted by each of the two models, OD^{sim1} and OD^{sim2}. As seen Fig. 6(a), the predicted optical depths were hardly changed by including the full time evolution: $\left|OD^{\mathrm{sim1}} - OD^{\mathrm{sim2}}\right| / OD^{\mathrm{sim1}} \leq 0.005$. Thus, for

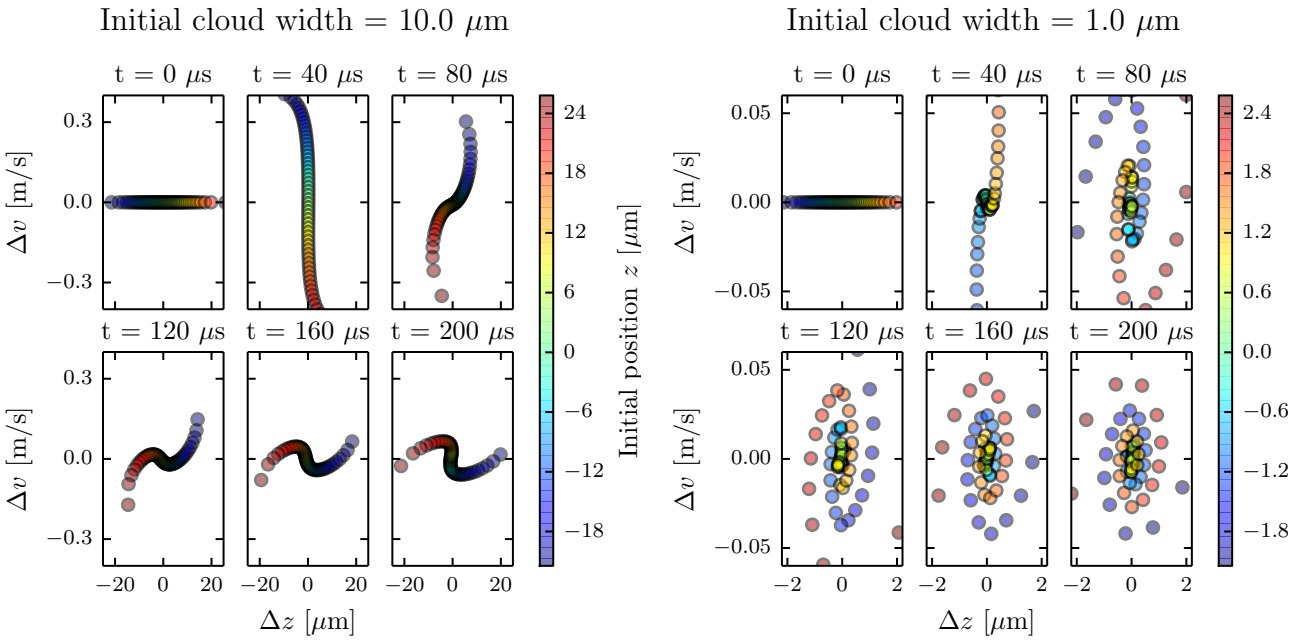

Figure 5: Phase space evolution of an atomic cloud exposed to probe light with intensity $\tilde{I}_0 = 1.2$. We defined $\Delta v = v - \langle v(t) \rangle$ and $\Delta z = z - \langle z(t) \rangle$, subtracting out the center of mass position and velocity of the cloud. The column density $\sigma_0 n$ is 1.6, and the initial cloud is a Gaussian with a width of 10 μm in (a) and 1 μm in (b). The center of mass velocities $\langle v \rangle$ are (0, 3.41, 5.26, 6.52, 7.50, 8.32) m/s sequentially, and are the same for both initial cloud widths.

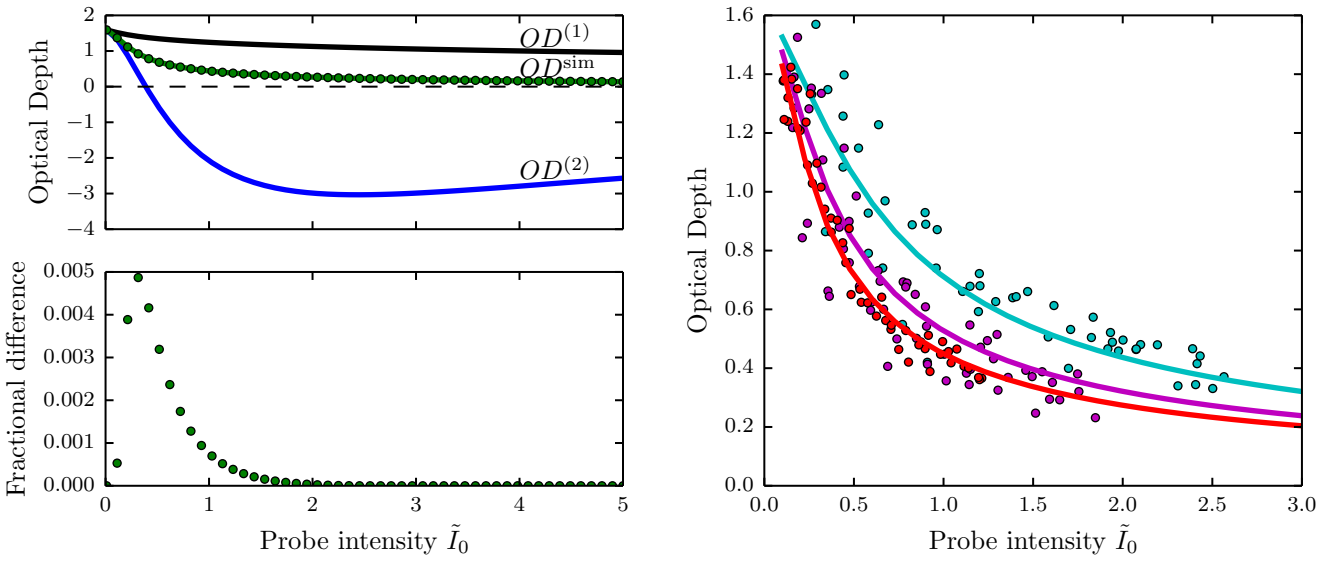

(a) (b)

Figure 6: (a) Top. Optical depth as a function of probe intensity for an imaging time $t = 100$ μs. $OD^{(1)}$ and $OD^{(2)}$ are optical depths predicted from a given column density by Eq. (2.4) and (**??**) respectively. The two versions of simulated optical depth, OD^{sim1} (green curve) and OD^{sim2} (green dots) are plotted. Bottom. The fractional difference between two versions of the simulated OD, $\left|OD^{\mathrm{sim1}} - OD^{\mathrm{sim2}}\right| / OD^{\mathrm{sim1}}$. (b) The optical depth as a function of probe intensity for three imaging times: $t = 40$ μs (cyan), $t = 75$ μs (magenta), $t = 100$ μs (red). The dots represent experimental data and the lines represent the best fit of simulated data. The optimal fit parameters pictured are a $\sigma_0 n$ of 1.627(5) and saturation intensity of 29(7) counts/μs.

the purposes of deducing the atom density from experimental optical depths, the stationary atom model is sufficient. Furthermore, we simulated a range of initial density profiles $\rho(z)$, and found their impact to be negligible – the only observable is the integrated atomic density $n = \int \rho(z)\mathrm{d}z$. Still, for interpreting experimental images, we used the data generated by the traveling atom simulation.

2.7 SNR optimization

This simulation allowed us to interpret experimental data. For a given imaging time, we created a look-up table of predicted optical depth as a function of probe intensity and atomic column density. We then found the observed optical depth on this table, with the given probe intensity, and inferred the atomic density. The uncertainty in the measured intensities can be propagated through this procedure, and we established optimal imaging parameters to maximize the SNR of this detection

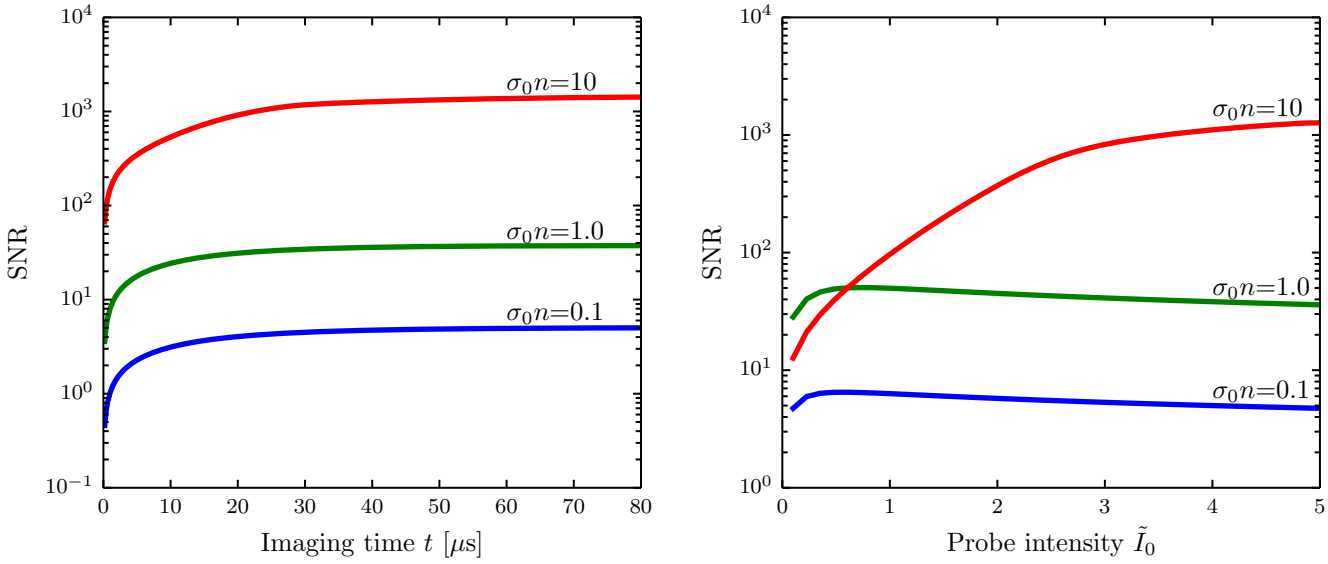

Figure 7: SNR for three different column densities after correcting for recoil induced detuning. (a) SNR as a function of imaging time for a probe intensity of $\tilde{I}_0 = 5.0$ and (b) SNR as a function of probe intensity for an imaging time of 50 μs.

scheme.

The only source of measurement uncertainty we considered was the Poisson noise on the detected arriving photons (i.e., photoelectrons) with standard deviation proportional to $q_e\sqrt{N_p}$, where q_e is the quantum efficiency of the camera and N_p is the photon number. We then propagated this uncertainty through our correction scheme to obtain the uncertainty in our deduced value of $\sigma_0 n$. We define the SNR as $\sigma_0 n/\delta_{\sigma_0 n}$, where $\delta_{\sigma_0 n}$ is the propagated measurement uncertainty.

As seen in Fig. 7(a), after about 40 μs extending the imaging time no longer yields appreciable improvement in SNR. Imaging for 40 μs as opposed to 10 μs where the uncorrected model is appropriate, improves the SNR by a factor of 1.5. We performed the experiments described in the second section at 40 μs imaging time. Figure 7(b) shows that the optimal probe intensity varies with the atomic column density. For low atom numbers, $\sigma_0 n \approx 0.1$, a probe intensity of $\tilde{I}_0 \approx 0.6$ is best. However, in our experiment the probe intensity had a Gaussian profile and was not uniform over the whole image. The typical probe intensities used in our experiments varied over the $2\tilde{I}_0 = 0.1 - 0.7$ range.

2.8 Calibration of saturation intensity

Our absorption images were taking using a charge-coupled device (CCD) camera. Each camera pixel converted the photons it was exposed to, with some efficiency, into photoelectrons, and digitally returned an integer, called 'counts', that was proportional to the radiant fluence. However, the proportionality constant depends on many factors, such as the quantum efficiency of the camera, the electronic gain during the readout process, losses in the imaging system and the polarization of the probe light.

We determined this proportionality constant through direct measurement. In the limit where the system is adequately described by $\sigma_0 n = -\ln(\tilde{I}_f/\tilde{I}_0)$, only the ratio of the initial and final intensities matter, and this proportionality constant is irrelevant. In all other regimes, however, the ratio of the initial and final intensities to the saturation intensity also comes into play, making the proportionality constant significant. One way to approach this calibration is to determine the saturation intensity in units of 'counts' per unit time.

To calibrate the saturation intensity in camera counts per unit time, we took absorption images of ^{40}K clouds at three different imaging times (40 μs, 100 μs, and 200 μs) with varying probe intensities. In a small region at the center of the cloud the atomic density was approximately uniform, and we averaged the initial and final intensities of each pixel in that region. Thus, for each image we obtained $\tilde{I}_0$ and $\tilde{I}_f$, in counts per microsecond. We then simultaneously fit our simulated optical depth OD^{sim} to this full data set, with the atomic density $\sigma_0 n$ and I_{sat} in counts per microsecond as free parameters. As seen in Fig. 6(b), the model produced a good fit to the experimental data, and provided a calibration of the saturation intensity for our experiment.

Bibliography

[1] H.J. Metcalf and P. van der Straten. *Laser Cooling and Trapping*. Graduate Texts in Contemporary Physics. Springer New York, 1999.

[2] G. Reinaudi, T. Lahaye, Z. Wang, and D. Guéry-Odelin. Strong saturation absorption imaging of dense clouds of ultracold atoms. *Opt. Lett.*, 32(21):3143–3145, 2007.

[3] G. O. Konstantinidis, M. Pappa, G. Wikstroem, P. C. Condylis, D. Sahagun, M. Baker, O. Morizot, and W. von Klitzing. Atom number calibration in absorption imaging at very small atom numbers. *Central European Journal Of Physics*, 10(5):1054–1058, 2012.

[4] Lindsey J. LeBlanc. *Exploring many-body physics with ultracold atoms*. PhD thesis, University of Toronto, 2011.